

Two-dimensional silicide 5×3 structure on Cu(001) as seen by scanning tunneling microscopy and helium-atom scattering

A. P. Graham*

*Cavendish Laboratory, Cambridge CB3 0HE, United Kingdom
and Department of Chemistry, Rutgers University, Piscataway, New Jersey 08855*

B. J. Hinch

Department of Chemistry, Rutgers University, Piscataway, New Jersey 08855

G. P. Kochanski

AT&T Bell Laboratories, Murray Hill, New Jersey 07974

E. M. McCash[†] and W. Allison

Cavendish Laboratory, Cambridge, CB3 0HE, United Kingdom

(Received 23 June 1994)

The incommensurate 5×3 structure, which is formed when silicon is deposited on copper(001) via a saturation exposure to silane at 420 K, has been examined with helium-atom scattering and scanning tunneling microscopy. The surface was found to be a two-dimensional copper-silicon alloy having large domains of a near perfect hexagonal structure with Cu_2Si stoichiometry. The surface layer displays a rotation of *one* surface-lattice vector with respect to the substrate of 4.4° , and a high-order commensuration along the other surface-lattice vector, *without* rotation. The overlayer exhibited unequal densities of the four possible domains and it appears that the long-range order is influenced by the presence of steps on the copper(001) surface. The overall atomic density in the surface layer is 27.6% higher than on the unreconstructed surface. The driving force for the formation of the sheared hexagonal structure is believed to be the need to increase surface coordination and density together with a strongly directional in-plane bonding between Cu and Si atoms.

I. INTRODUCTION

The properties and performance of metal-semiconductor interfaces is of fundamental importance to the semiconductor industry. It has been shown that the microscopic structure of both metal-semiconductor interfaces and silicide-silicon interfaces can control the measured Schottky barrier heights.¹ Although copper has not been used to date for interface formation due to its high solubility in silicon, stable copper silicide-silicon interfaces have potential applications for electrical contacts² and for Schottky barrier-type photovoltaic cells. Incidentally, copper silicide has also been studied as an intermediate in the formation of ultrapure silicon^{3,4} suitable for solar cell applications.

Research effort has concentrated on the growth of copper on silicon surfaces. The initial stages during the growth of copper on silicon(111) have proved difficult to analyze due to the complex structures with poor long-range order formed at monolayer coverage.⁵⁻⁹ The deposition of silicon on copper(001) via the chemical-vapor deposition of silane (SiH_4) turns the copper-silicon interface "upside down." The resulting interface exhibits a microscopic structure with long-range order, in contrast to that formed by deposition of Cu on silicon. We can anticipate very different Schottky barrier diode characteris-

tics for devices grown in these two ways.

Chemical-vapor deposition (CVD) using silane for deposition of silicon on copper(001) is an attractive route for the study of copper-silicon interfaces. Chemical-vapor deposition from silane deposits clean, unclustered silicon atoms on the copper surface following dehydrogenation of the silane at copper surface temperatures above 300 K.¹⁰⁻¹³ When silicon is deposited on copper(001) via a saturation exposure to silane at 400 K, an incommensurate 5×3 electron-diffraction pattern is observed.¹⁰ Dubois and co-workers suggested that the silicon had been incorporated into the copper surface layer, which consequently reconstructed into a hexagonal structure. In the present study, we aim to elucidate the precise nature of the copper-silicon interface formed by CVD of silane at 420 K using two uniquely surface sensitive techniques, helium scattering and scanning tunneling microscopy.

II. EXPERIMENT

The helium scattering experiments were undertaken in a purpose built, ultrahigh vacuum chamber¹⁴ utilizing a Campargue-type atom beam source,¹⁵ and both fixed angle and moveable differentially pumped quadrupole mass-spectrometer detectors. The moveable detector allows a large range of scattering conditions to be used at

an angular resolution of 0.44° , while the fixed angle detector permits high-resolution (0.2°) diffraction spectra to be taken for precise measurement of diffraction peak positions. A six axis UHV manipulator permitted precise positioning of the sample with respect to the incoming helium beam and backscattered helium detectors.

The copper(001) sample was cut from a single-crystal rod to $<0.5^\circ$, mechanically and chemically polished before insertion into the vacuum chamber. In vacuum, the sample was cleaned using cycles of ion bombardment ($3 \mu\text{A cm}^{-2} \text{Ar}^+$ at 1 kV) and annealing to 700 K until only a constant narrow, intense, specular helium scattering peak was observed in the diffraction spectra. Low-energy electron diffraction confirmed the high degree of order of the copper(001) surface showing a sharp 1×1 diffraction pattern with low diffuse background. Ion bombardment and annealing were carried out prior to each exposure of the copper surface to silane. Silane exposure was carried out at 10^{-6} mbar (total measured pressure) using a 0.5% silane in argon mixture. The exposures quoted have been corrected for the ionization gauge sensitivity to argon and the silane gas dilution.

The STM experiments were performed in an ion pumped UHV chamber equipped with a room-temperature scanning-tunneling-microscope low-energy-electron-diffraction (LEED), ion sputtering gun, and electron bombardment sample heating facilities.¹⁶ The STM tungsten tip was cleaned prior to each experiment on the copper surface using field emission of electrons from the tip to a platinum sample ($1 \mu\text{A}$ at 200–300 V for up to an hour). The same copper sample was used for the helium scattering experiments and STM experiments, and was cleaned using cycles of ion bombardment ($200 \mu\text{A cm}^2 \text{Ne}^+$ at 1 kV) and annealing at 700–800 K. Low-energy-electron-diffraction was also used to confirm the high degree of order of the copper(001) surface showing a sharp 1×1 diffraction pattern with low diffuse background. Silane exposure was carried out at 10^{-6} torr (total measured pressure) using a 1.0% silane in helium mixture. The exposures quoted were corrected for the ionization gauge sensitivity to helium and the silane gas dilution. Upon saturation of the surface to silane, at surface temperatures above room temperature, the resulting structure shows no noticeable further contamination. This would indicate that at 10^{-10} torr the average sticking coefficient of residual background gases is negligible.

III. HELIUM SCATTERING RESULTS AND DISCUSSION

A helium diffraction spectra following a saturation silane exposure at 420 K is shown in Fig. 1. The diffraction scan was taken using the fixed helium detector along the (110) azimuth for a fixed total scattering angle of 88° following cooling of the sample to 170 K from the exposure temperature of 420 K. The strongest peak in the diffraction spectrum is the specular reflection at 0° sample tilt ($\theta_i = \theta_f = 44^\circ$). The next most intense peaks in the diffraction spectrum, at saturation exposure, correspond approximately to a $5a$ surface periodicity. The weakest diffraction features correspond to a $13a$ periodi-

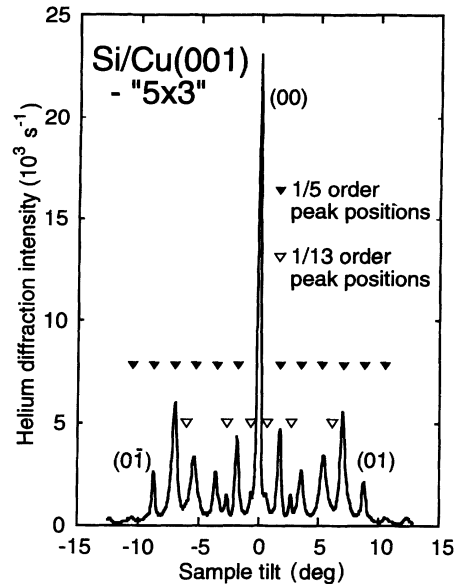


FIG. 1. A helium diffraction scan from the copper(001) surface following saturation exposure to silane at 420 K. The sample temperature was 170 K with 66-meV beam energy. The scattering angle was fixed at 88° and the scan was obtained by tilting the (001) surface normal out of the scattering plane while maintaining the (110) vector in the scattering plane. The central peak corresponds to specular scattering.

city, and are seen as select $\frac{1}{13}$ order peaks including $\frac{1}{13}$ peaks either side of the specular peak, and $\frac{4}{13}$ peaks at $\pm 2.8^\circ$. In addition, there are shoulders on the $\frac{5}{13}$ peak at 6.0° suggesting the presence of a $\frac{2}{13}$ peak. The majority of the $\frac{1}{13}$ order intensity is found close to the $0, \frac{1}{3}, \frac{2}{3}$ diffraction conditions, thus explaining the old assignment of the structure as (5×3) .

The strongest nonspecular diffraction peaks "move" towards the $5a$ diffraction positions as the silane exposure is increased towards saturation.¹³ The adjustment in position of these diffraction peaks with exposure strongly suggests that the copper-silicon structure which is forming on the surface is compressing with exposure and is not commensurate with the copper(001) lattice, i.e., the surface lattice of the surface structure does not match precisely with the underlying copper crystal structure. The nature of this incommensuration will be discussed later.

There are a number of aspects of the helium diffraction pattern which give clues as to the structure of the surface. Helium scattering observes the corrugation arising primarily from the outermost density of states $\rho(r)$ for the surface structure.¹⁷ Hence the periodicities observed cannot arise from a subsurface reconstruction, but must originate within the surface layer. A key feature of the helium diffraction scan is the arrangement of intensity into the various diffraction peaks. A high corrugation, such as that created by atoms sitting on the surface, tends to promote intensity in diffraction peaks further away from the specular reflex, in addition to decreasing the in-

tensity in the specular reflex itself. For the opposite case, a low corrugation promotes intensity in peaks close to the specular reflex only, and maintains a high specular reflectivity. In the current study, the diffraction intensity is contained within a $\pm 9^\circ$ angular range of the specular reflex, suggesting a small surface corrugation. Such a small corrugation can only be caused by incorporation of the silicon atoms into the copper surface. It is possible to rule out adsorption sites above the surface plane.

Figure 2 shows a more complete helium diffraction pattern derived from a number of diffraction scans taken through the various diffraction peaks observed. In this figure, the peak positions are indicated as a function of K_x and K_y . The scattered intensities are indicated by the respective diameters of the diffraction spots. The diffraction pattern shows that the surface is constructed from two domains of an unusual 5×13 structure where the $5a$ surface corrugation is significantly stronger than for the $13a$ periodicity. We will therefore address the nature of the $5a$ periodicity first.

A $5a$ periodicity in the surface layer is quite unusual for a surface as unreactive as copper. However, a number of other surfaces have displayed a $5a$ periodicity, which is now typically associated with a hexagonal reconstruction of a surface above a square subsurface lattice, as

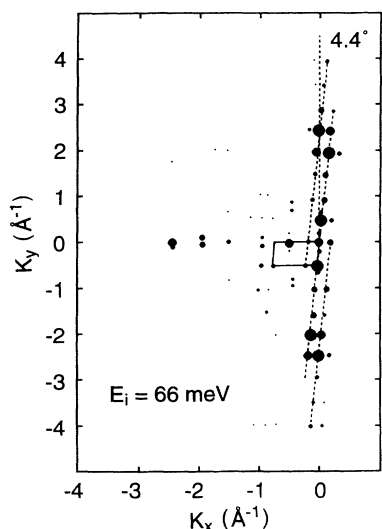


FIG. 2. Two quadrants of the helium diffraction pattern from the 5×3 reconstruction of copper(001) following a saturation exposure of silane at 420 K. The pattern was constructed from a series of diffraction scans similar to Fig. 1 for a beam energy of 66 meV and a sample temperature of 170 K. The angle of incidence at $K_y = 0$ was 26° . The size of the spot on the pattern indicates the intensity observed in the diffraction peak. The peaks arising from each domain are split in one direction only. The angle that the split diffraction peaks make with the copper substrate is 4.4° , which is consistent with the $13a$ periodicity observed. Note that one domain is preferred above the other three possible domains, indicating that steps play a major role in the growth of the overlayer structure. An approximate 5×3 unit cells is shown in the diagram.

observed on Pt(100),¹⁸⁻²⁰ Ir(100),²¹⁻²³ Au(100), and W(100).^{24,25} We suggest, therefore, that the $5a$ periodicity in the present helium diffraction pattern arises from a hexagonal reconstruction of the copper surface as shown in Fig. 3. Note that pure copper does not display this reconstruction, unlike gold, but might be induced to do so by a low proportion of silicon in the surface layer. The presence of the $5a$ periodicity does not, however, indicate the position or quantity of silicon atoms in the surface layer, and therefore we must analyze the $13a$ periodicity to provide some additional information on the surface layer structure.

The second, weaker, corrugation seen in the diffraction scan corresponds to a $13a$ surface periodicity. Only $\frac{1}{13}$, $\frac{4}{13}$, and $\frac{9}{13}$ peaks are observed for a room-temperature helium beam (66 meV). Apart from the $\frac{1}{13}$ peak, the other peaks observed with a $13a$ periodicity fall close to third-order diffraction peak positions. The fact that only these peaks are displayed in the diffraction scan, and none of the other possible 13th-order peaks are seen, indicates that the form factor for the 5×13 unit cell has a strong $3a$ periodicity in this direction. That is, the surface corrugation has a periodicity of *approximately* $3a$ but the surface-lattice vector, which determines the possible Bragg diffraction positions, has a periodicity of $13a$. The reason for the difference will be discussed shortly. The 13th-order diffraction peaks have intensity which is much smaller than those observed for the fifth-order peaks indicating that the corrugation along the $13a$ direction, of predominantly $\sim 3a$ nature, has a much smaller amplitude.

Having established that the largest component of the surface corrugation in the $13a$ direction is close to a $3a$ periodicity, it is important to ascertain why this should be the case. The presence of the fifth-order diffraction peaks indicates that the surface has undergone a hex reconstruction but they do not indicate where the silicon atoms are in the reconstructed surface layer. Remembering that the silicon has been incorporated into the surface layer, the weak 13th-order, or $3a$ corrugation features, can be assigned to a corrugation difference between silicon and copper atoms in the surface layer as seen by the helium atoms. The most natural way to produce a $3a$ corrugation on the hex lattice is to replace every third surface atom in an ordered array with a second atomic species as demonstrated in Fig. 3. The route is equally applicable to silicon *or* copper being the majority atomic species in the surface layer, i.e., the surface layer can be Cu_2Si *or* CuSi_2 . However, a study of silane adsorption on Cu(111) suggested a one-third monolayer coverage of silicon and we can conclude that the surface in the present study is Cu_2Si .¹¹ This conclusion is supported by STM topographs of copper island formation (discussed below). It is interesting to note that the resulting hexagonal overlayer structure shown in Fig. 3 also explains the $(\sqrt{3} \times \sqrt{3})R 30^\circ$ structure observed on Cu(111) (Refs. 11 and 12) and Ni(111),²⁶ where no detailed structural study has yet been performed.

So far, in discussing the surface corrugation resulting from the incorporation of silicon atoms into the surface, the origin of the $13a$ periodicity has not been considered.

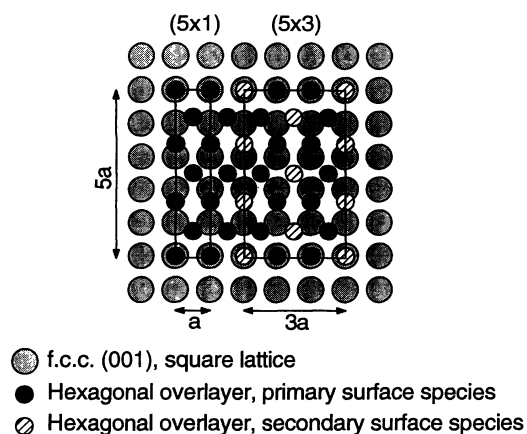


FIG. 3. Schematic representation of the hexagonal (hex) reconstruction on a square substrate. The hexagonal lattice almost matches with the square lattice after five lattice spacings. Hence a $5a$ periodicity would be observed by LEED and helium scattering. The $\sim 3a$ periodicity can be constructed by replacing every third surface atom with a different atomic species as shown.

Several interesting features are demonstrated by the helium diffraction pattern for the two quadrants shown in Fig. 2. First, there is a clear preference for one particular domain orientation over the other possibilities. The result is that diffraction intensity is concentrated along the K_y axis instead of equally along the K_x and K_y axes. Second, the peaks are split *perpendicular* to the axis on which they lie. The splitting corresponds to $13a$ for each fifth-order peak and the split peaks line up with a lattice vector rotation of 4.4° ($\tan^{-1}[\frac{1}{13}]$). The 5×3 unit cell for one of the domains is drawn on the diffraction pattern, although the correct peak assignments are difficult for diffraction peaks away from the major axes. We conclude that four different sheared 5×13 unit cells or domains can exist. However, due to the properties of the substrate, some domains grow preferentially to others.

The domain preference can arise from the effect of surface steps produced by a surface miscut in manufacture. The quoted miscut is less than $< 0.5^\circ$ suggesting that the terrace lengths should be greater than 300 \AA on average. Therefore, the domains formed by the surface reconstruction must be of the order of 200 \AA or larger to be affected by the step orientation. Such terrace and domain sizes are consistent with STM images. Fortunately the domain preference makes the analysis of the lattice vector rotation easier as only one set of diffraction positions is effectively observed. The splitting of the fifth-order diffraction peaks along one high-symmetry direction, observed in the diffraction pattern, indicates that only the $13a$ lattice vector, and not the $5a$ vector, is rotated by 4.4° with respect to the Cu(001) substrate. Figure 4 shows a structural model that is consistent with the data. The $13a$ periodicity originates from the *equivalent sites* for silicon atoms after translation by 13 copper substrate lattice

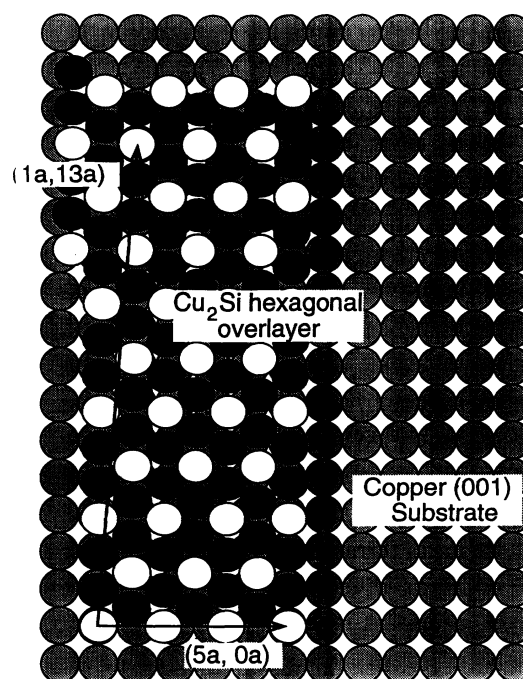


FIG. 4. Schematic diagram showing the proposed structural model of the surface layer together with the origin of the $13a$ periodicity and the 4.4° rotation. Note that the $5a$ direction is *not* rotated with respect to the copper substrate.

spacings along the copper rows, and one lattice spacing in the $5a$ direction. The structure is produced by shearing a 5×3 unit cell by 0.73° with respect to the copper(110) direction. The shear will naturally produce a significant corrugation amplitude for the $13a$ surface periodicity which results in a high $\frac{1}{13}$ -order diffraction peak intensity. Essentially, the $3a$ corrugation is maintained, except that the silicon sites are not equivalent and therefore the Bragg diffraction conditions are not determined by the $3a$ periodicity. The origin of the 13th-order periodicity has a marked similarity to that shown on a clean ("hex") surface reconstruction of Pt(100),¹⁸ although we shall demonstrate that the silicide structure is not the same as the Pt(100) $R0.73^\circ$ phase.

In addition to the rotation observed for the $3a/13a$ axis, an incommensuration in the $5a$ direction was observed during silane dosing.¹³ The Bragg diffraction positions were observed to move as silane exposure was increased. The only way that the diffraction peaks can move is if the lattice spacing which determines them is changing. The conclusion from this observation is that the copper silicon overlayer periodicity is developing independently from the copper substrate lattice spacing, in other words, the overlayer is incommensurate with the substrate. The nature of the incommensuration is not a lattice vector rotation because split peaks parallel to the $5a$ axis were not observed in diffraction from the surface (Fig. 2). The incommensuration is therefore parallel to the substrate copper lattice vector.

A high-resolution, fixed angle detector was used to determine the exact positions of the “fifth-order” diffraction peaks. For diffraction for a high-order commensurate (HOC) surface, the diffraction peaks are expected to have unequal spacing along the “incommensurate” lattice vector.²⁰ The unequal spacing arises from an interference between the form factor of the surface which depends upon the surface corrugation, and the structure factor which depends upon the length of the unit cell (Bragg condition). The resulting interpeak maxima spacings reflect the interference and can be used to determine the HOC lattice repeat length. The data indicate that the (5×3) unit cell is expanded (very slightly) with respect to the ideal (5×3) structure and that the smallest HOC unit cell size, which is consistent with experiment, is 157 ± 5 copper lattice spacings. The unit cell corresponds to an average length scale of 400 ± 13 Å. This HOC unit-cell size is greater than the minimum estimate of the mean terrace length, consistent with the STM observation that domains frequently cross steps. However, the diffraction peaks following silane exposure are broader along the $5a$ direction than the experimental resolution of the helium diffractometer suggesting that some domains are much shorter than this average length. The observed peak widths (full width at half maximum) are in excess of the separation of peak maxima positions from ideal $\frac{1}{5}$ -th-order positions; indicating that clearly there are still some domains which have a net expansion with respect to the ideal five times periodicity. The lack of a sharp higher-order periodicity is thus indicative of a superstructure that is highly susceptible to pinning (probably in registry with surface defect structures).

In conclusion, the copper-silicon surface exhibits helium diffraction features that are compatible with a hex reconstruction of the surface-atom layer. The predominant corrugation observed is 5×1 , where the corrugation amplitude in the $5a$ direction is estimated as 0.5 -Å peak from the helium diffraction intensities. The corrugation arises from two components. A minor component comes from the different effective sizes of copper and silicon atoms within the hexagonal surface layer. A more important component is due to the rumpling of the surface film as it lies in contact with a substrate of a different periodicity. The hexagonal restructuring extends one atomic layer deep only, otherwise the $5a$ periodicity diffraction features would not be observed. Every third atom on the surface is different leading to a $3a$ diffraction periodicity, and the conclusion that the surface is Cu_2Si ($\theta_{\text{Si}} = 0.4$) in composition. Two different types of “incommensuration” are displayed by the surface. In the $3a$ direction the atom rows are sheared by 0.73° leading to an additional $13a$ periodicity in the surface structure. The corresponding lattice vector is inclined by 4.4° with respect to the substrate. In addition, in the $5a$ direction, the surface exhibits a high-order commensurate structure with an average repeat distance of approximately 400 Å. The surface primitive lattice can therefore be described by the matrix:

$$\begin{bmatrix} 13 & 1 \\ 0 & 157 \end{bmatrix} \approx \begin{bmatrix} 13 & 1 \\ 0 & 5 \end{bmatrix}.$$

IV. SCANNING-TUNNELING-MICROSCOPY RESULTS AND DISCUSSION

In contrast to helium diffraction, STM images the surface in real space, which should permit a “direct” observation of the surface structure.²⁷ However, in the present study, the surface layer contains two different atomic species that have very different electronic properties, so care must be taken in the interpretation of the STM topographs. The copper(001) surface was prepared with a saturation exposure of silane at 420 K and cooled to room temperature (300 K) prior to STM experiments.

Figure 5 presents a large area topographic scan of the copper-silicon surface indicating the size and degree of order of the copper-silicon domains that can be formed. At 3 V and 0.2 nA the STM tip is too far away from the surface to resolve single atoms on the surface, and therefore the topograph displays only the longer-range corrugations present in the surface. The “stripes” observed in the topograph are ~ 13 Å apart ($\sim 5a$ where a is the copper substrate lattice spacing) and have a corrugation of 0.3 Å. The $5a$ stripes reflect the modulation of the surface layer by the substrate due to a difference in structure. Scanning tunneling microscopy observes the same strong $5a$ periodicity observed in the helium diffraction

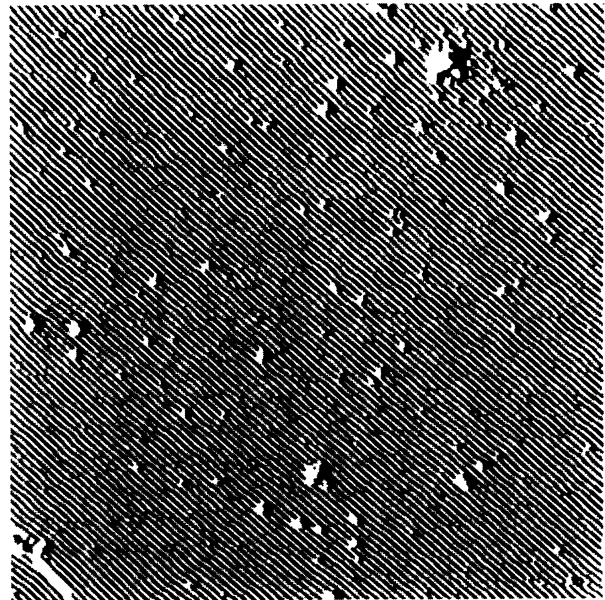


FIG. 5. A topograph of the surface following silane exposure to saturation at 420 K. The image was taken at a tunneling current of 0.2 nA and a sample bias of $+3.0$ V. The topograph is approximately 1160 Å across and has not been corrected for thermal drift of the STM during measurement. The topograph shown is the first derivative of the height data across the picture, i.e., dz/dx , where the height data has been convoluted with a 3.0 -Å-wide Gaussian smoothing function before taking the derivative. Regions of positive slope are shown as bright, whereas regions of negative slope are shown as dark. The topograph shows one domain of the copper-silicon overlayer extending 1500 Å. The small islands on the topograph are probably copper that has been deposited from the tunneling tip.

and LEED patterns from the same surface. The longer range HOC periodicity observed by helium scattering in the $5a$ direction cannot be seen in the surface topographs taken with STM. However, it is interesting to note that the surface layer is apparently continuous; that is, the incommensuration observed using helium scattering appears not to rise from sharp phase shift walls, domain boundaries or surface stress relief dislocations. Such an observation adds weight to the idea that the copper-silicon intralayer bond is very strong, and that the hexagonal overlayer is only weakly modulated by the substrate.

The random defects observed in the topograph are possibly due to spare copper released from the surface during formation of the overlayer, or more likely, copper clusters deposited from the tip.²⁷ Experimentally, we found it was possible to deposit material with larger sample biases while the copper silicon overlayer around the clusters remains undisturbed. Copper is deposited typically when the sample bias is ≥ 2 V. Negative sample biases were rarely used during topographic scans as this was found to increase the noise in the images dramatically, obscuring any topographic features previously observed using positive sample biases. This noise level also obscured the signal observed during IV scans preventing a reliable electronic analysis of this surface.

The topograph shown in Fig. 6 has been taken over a smaller area of the saturated surface. There are two, new, weaker periodicities evident in the domains, running approximately perpendicular to the $5a$ "stripes." One corrugation is along the $5a$ stripes (0.1-Å amplitude peak to peak) and has a short wavelength of 7.7 Å ($\sim 3a$) while the other periodicity (0.1-Å peak to peak) has a longer 33.5-Å wavelength ($\sim 13a$). The amplitude of the $3a$ periodicity can be attributed to an electronic difference between the copper and silicon present in the surface. Such low corrugations cannot arise from silicon atoms sitting on top of the copper surface, but must originate with silicon atoms incorporated into the surface layer. The $5a$ corrugation, measured perpendicular to $5a$ stripes, in this topograph is 0.45 Å.

The upper right-hand corner of Fig. 6 also displays the abrupt termination of the striped structure in a domain boundary. The adjacent continuous stripe of one domain is apparently unaffected by the proximity of the next domain. This indicates that there can be only a very narrow strained region between domains.

By lowering the sample bias to 0.5 V and increasing the tunneling current in 1 nA it is possible to move the tip closer to the surface and obtain a higher-resolution topograph of the surface (Fig. 7). The 5×3 unit cell is evident, but, in addition, it is possible to observe more detail within that unit cell. By deemphasizing the variation in topographic height due to the $5a$ corrugation [Fig. 7(b)], it is possible to plot the position of the tunneling features with the strongest atomic scale corrugation. The positions fall on a hexagonal mesh with a side length of 4.4 Å ($\sim \sqrt{3}a$) with six complete high features per 5×3 unit cell. Therefore, the surface layer is definitely hexagonal, and the topograph displays its highest points for the minority surface component, which we propose are silicon atoms in the surface plane.

By following a line of silicon atoms parallel to an individual $5a$ "stripe" we can see that the direction of the line of silicon atoms deviates away from the stripe direction. There is a match of topograph height for these locally high features after 13 atoms indicating that the " $3a$ " surface layer lattice vector is rotated with respect to the substrate atoms. However, due to the intrinsic inaccuracies involved in taking STM topographs, namely, thermal drift and piezo crystal creep, it was not possible to determine the angle between the $5a$ lattice vector and the $13a$ lattice vector accurately. Hence, in the present experiment, the STM could not determine the difference between the unit-cell matrices:

$$\begin{bmatrix} 13 & 0 \\ 0 & 5 \end{bmatrix} \text{ and } \begin{bmatrix} 13 & \pm 1 \\ 0 & 5 \end{bmatrix}.$$

From Fig. 6 we can see that the $5a$ direction surface-lattice vector is not rotated with respect to the substrate to within the accuracy of the STM topograph. The corru-



FIG. 6. A topograph of the surface following silane exposure to saturation at 420 K. The image was taken at a tunneling current of 0.1 nA and a sample bias of +2.0 V. The topograph is approximately 190 Å across and has been corrected for thermal drift of the STM during measurement. The topograph shown is the first derivative of the height data across the picture, i.e., dz/dx , where the height data has been convoluted with a 0.5-Å-wide (sigma) Gaussian smoothing function before taking the derivative. Regions of positive slope are shown as bright, where as regions of negative slope are shown as dark. The strongest corrugation on the copper-silicon structure is the $5a$ periodicity (stripes). Within each strip, the $3a$ periodicity can be seen, with a $13a$ periodicity observed as a modulation of the $3a$ periodicity height along the stripe. The dark band in the top left-hand corner of the topograph is a surface step.

gations measured by the STM under these conditions are larger than those measured with higher sample biases and lower tunneling currents. The $5a$ corrugation in this topograph has a peak-to-peak height of 0.9 \AA , while a $3a$ corrugation has a peak-to-peak height of 0.8 \AA and the $13a$ periodicity has a corrugation of 0.1 \AA . The difference between the values obtained for this topograph, and those presented earlier, will be discussed in the next section.

The STM can also be used to estimate the quantity of silicon included in the surface layer. Incorporating sil-

icon into the surface necessitates the removal of copper atoms from the surface. In the topographs shown in Figs. 6 and 7 there is no evidence of this surface copper, and from this we can conclude that during growth the copper has diffused to a step edge where it has become incorporated into the step. By reducing the diffusion length of the copper during the formation of the copper-silicon layer, the system will not be able to reach such an equilibrium and the copper will remain on the open terrace. The diffusion length of the copper atoms can be reduced by decreasing the temperature at which silane is

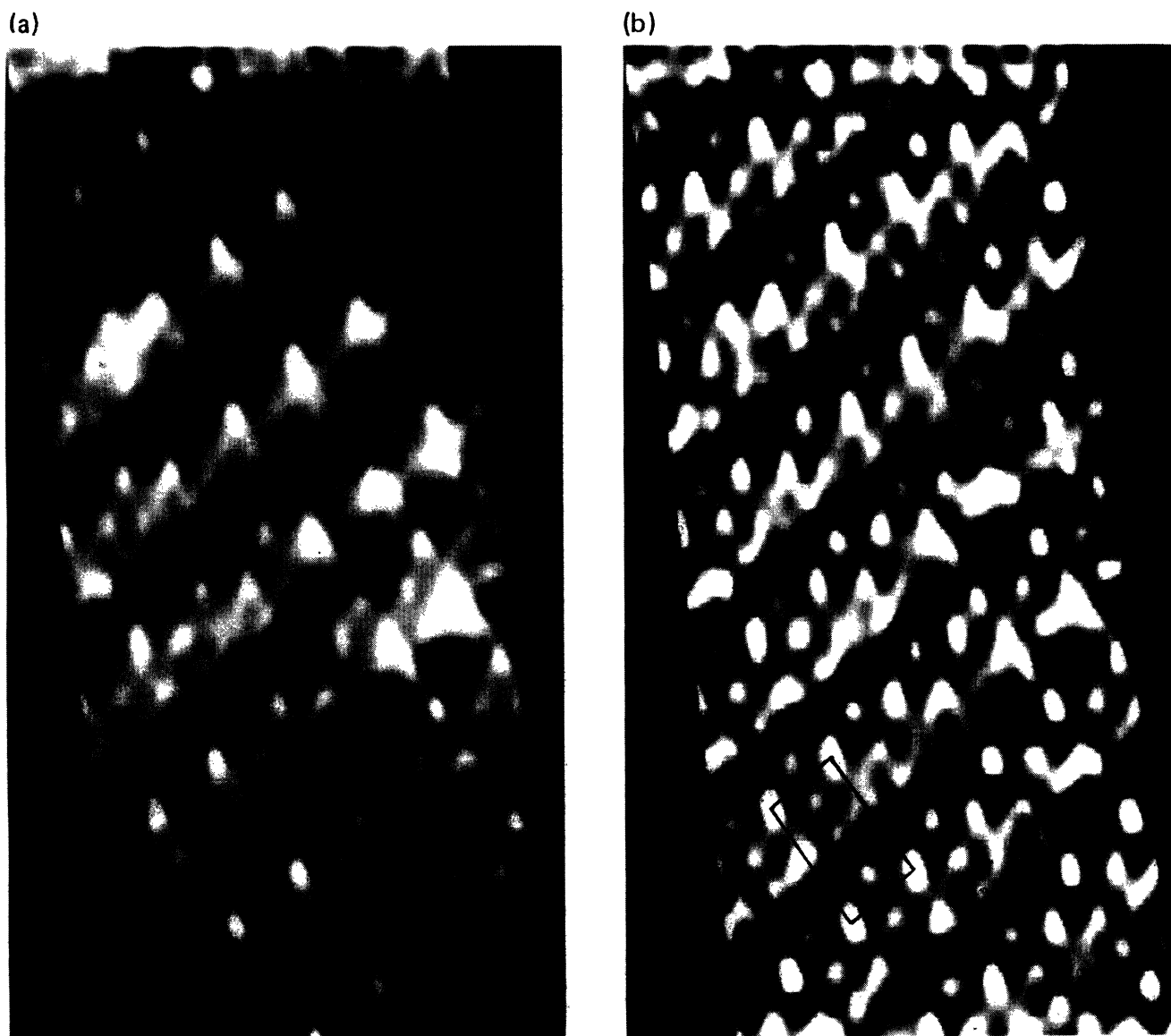


FIG. 7. A topograph of the surface following silane exposure to saturation at 420 K. The image was taken at a tunneling current of 1.0 nA and a sample bias of $+0.5 \text{ V}$. The topograph is approximately 46 \AA across and has been corrected for thermal drift. The most probable fit plane to the height data has been subtracted, and the data presented in two ways: (a) with the brightness representing the height, emphasizing the long-wavelength corrugations (5×3), and (b) with the brightness representing the local height (height relative to a 2-\AA Gaussian-weighted average of the vicinity). The 5×3 unit cell is shown on the latter topograph. The highest topographic features on the surface lie in sites consistent with the minority surface species in a hexagonal overlayer structure. Hence the high features can be assigned to silicon atoms in the overlayer.

adsorbed. Figure 8 is a surface STM topograph following a saturation exposure of the copper(001) surface to silane at 300 K instead of 420 K. In addition to the production of islands on the surface, the size of copper-silicon domains has been reduced. The growth kinetics of this system will be discussed elsewhere.²⁸

From the area of islands on an open terrace away from steps an estimate can be made about the quantity of copper released from the surface. To determine the amount of copper released it is necessary to take into account that the copper islands react with silane forming the copper-silicon structures that are only *one layer deep*. There is no experimental evidence for a covered or buried silicide layer over any small fracture of the surface. In Fig. 8, the *island area coverage* is 0.20 ± 0.02 . For the 5×3 hexagonal overlayer structure, with 18 atoms per 5×3 unit cell this island area corresponds to a *silicon coverage* of 0.40 ± 0.04 with respect to the copper substrate. Such a coverage is in agreement with an overlayer of Cu_2Si as originally proposed by Dubois and Nuzzo¹⁰ and consistent with the helium scattering results presented in the previous section as well as with the LEED diffraction and Auger spectra observed for the interaction of silane with copper(111).^{11,12}

Although a noticeable domain preference was observed during the helium diffraction experiments, none was evident in the STM topographs obtained for the silane saturated and subsaturation copper(001) surfaces. Such a

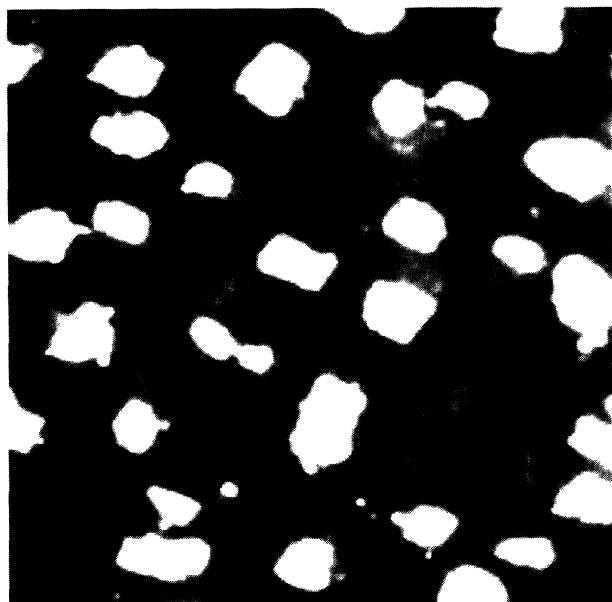


FIG. 8. A surface topograph following saturation silane exposure at 300 K. The image was taken at a tunneling current of 0.2 nA and a sample bias of 1.0 eV. The topograph is approximately 1050 Å across by 800 Å high and has not been corrected for thermal drift of the STM during measurement. The height data has been convoluted with a 1-Å-wide Gaussian smoothing function. The topograph shows part of a single terrace. The highest features on the terrace are the islands formed from the excluded copper.

difference may be attributed to a difference between the sampling scale for STM and helium scattering experiments, 10^4 Å for STM compared with 10^7 Å for helium scattering. Also, there is no guarantee that the STM and helium scattering experiments were centered on the same part of the copper(001) sample and sample preparation conditions (e.g., growth temperature) could not be identical within both apparatuses.

One interesting feature of STM is the ability to observe rare, small scale crystal features which manifest themselves on the surface corrugation, and cannot be seen by any other surface sensitive technique. An example of this is the screw dislocation presented in Fig. 9, which was observed at slightly less than saturation exposure. The screw dislocation produces the single layer step observed at the top right of the topograph. Note that the copper-silicon overlayer is distorted minimally around the step, further indicating the strength of the copper-silicon intralayer bond.

In conclusion, the STM results confirm that the copper-silicon surface has a hexagonal structure with Cu_2Si stoichiometry. The surface displays three periodicities, a large $5a$ corrugation corresponding to the lattice mismatch between the hexagonal overlayer and the square substrate, a weaker $3a$ periodicity corresponding to a difference in electronic properties between the copper and silicon in the surface, and a $13a$ periodicity which arises from a rotation of the " $3a$ " lattice vector with respect to the copper substrate.



FIG. 9. A topograph of the surface following 8 L silane exposure at 420 K. The image was taken at 0.25 nA and +0.5 V. The topograph is approximately 280 Å across by 280 Å high and has not been corrected for thermal drift. The height data have been convoluted with a 0.5-Å-wide Gaussian smoothing function. A screw dislocation is faintly circled at the top center of the topograph. Note the minimal distortion of the overlayer lattice around the dislocation.

V. COMPARISON OF TECHNIQUES

In the current study we have investigated a complex surface structure using two very powerful surface sensitive techniques. Scanning tunneling microscopy and helium-atom scattering (HAS) are both probes of the surface structure that generate a corrugation derived from structure within the electronic wave functions which extend far from the surface. This allows for a more enlightening comparison than would be possible with techniques that probe inner-shell electronic states, such as surface-extended x-ray-absorption fine-structure or x-ray scattering.

Helium atoms experience a long-range attractive interaction with the surface caused by the van der Waals interaction, followed by a shorter-range, stronger, repulsive interaction due to electron repulsion between the helium atom electronic states and those in the surface. Most of the structural information contained within the helium diffraction pattern is the result of the strong repulsive interaction, as the effect of the longer-range van der Waals interaction averages out over the surface.¹⁷ Thus surfaces can often be treated well within the hard wall approximation for high helium atom energies, where the helium atoms are effectively scattered from a hard corrugated surface. In the case of helium scattering, it is usually assumed that the corrugation observed depends upon the electronic wave functions that penetrate furthest out into the vacuum, in other words, the filled electronic states of the surface close to the Fermi level and that the effective corrugation is only weakly dependent on the incident energy. The maximum electron densities probed by the He atom are of order 10^{-4} per atomic volume.²⁹

Scanning tunneling microscopy, on the other hand, can probe both the filled and unfilled electronic states of the surface depending on the sample bias applied during the experiment.³⁰ In addition, the tunneling current (and sample bias) determine the overlap between the electronic wave functions of the tip and surface. For a fixed sample bias, as the tip gets further from the surface, the wave function overlap becomes smaller, and the tunneling current decreases. The topographic images obtained with the STM therefore change with a variation in tip bias and tunneling current.

For small negative sample biases ($\ll 1$ eV), the STM is probing the filled electronic states of the surface close to the Fermi energy just as those probed by thermal energy helium atoms scattering from the surface. The tunneling distance, which is controlled by the tunneling current for a fixed sample bias, determines the degree of wave function overlap in the same way that the incident-beam energy in helium scattering experiments determine the maximum degree of overlap (obtained at the turn around point) between the electronic states in the helium atom and those in the surface. Hence in this regime, helium scattering and STM should observe similar surface corrugation features. For larger, negative sample biases, the tunneling from a metallic surface is still dominated by the electronic states close to the Fermi energy, but additional deeper lying states are also probed. Therefore, as the

sample bias is increased, the corrugation observed by STM can deviate from that observed by helium scattering depending on the structure of the electronic density of states in the tip and surface. Naturally, there is not a direct analogy for positive sample biases, where the STM is probing the unfilled electronic states of the surface above the Fermi energy, with which the helium atoms interact relatively weakly.³¹

For a direct comparison of STM with He scattering, we can estimate the order of magnitude of electron density that the tunneling STM tip samples as follows. Imry and Landauer³² have pointed out that an ideal one-dimensional metal channel connecting two large metal objects will have a resistance of $\pi\hbar/e^2 = 12\,900\ \Omega$. As a STM that produces an image with atomic resolution cannot be tunneling over an area much larger than one atom, the conductivity will approximate that of the one-dimensional channel, with an additional factor of the probability that an electron will tunnel from the tip to the sample. This probability is $P = \exp(-\kappa z)$, where z is the tip height and κ is the spatial decay rate of the electronic wave functions (typically $\kappa \sim 20\ \text{nm}^{-1}$). The exponential dependence of the tunneling probability is the same as the decrease in the electron density, as one moves away from the surface. We can then calculate P as $P = \pi\hbar/(e^2 R)$, where R is the resistance of the tunnel junction, and thus the electron density as $\rho = P \times (\text{one conduction electron per atomic volume})$. For low-current STM operating parameters of 10 pA and 1 V ($10^{11}\ \Omega$), we sense the surface at $\rho = 10^{-7} e^-$ per atomic volume, and for high current operating parameters of 10 nA and 0.1 V ($10^7\ \Omega$), we sense the surface at $\rho = 10^{-3} e^-$ per atomic volume.

As indicated above, in STM the lateral resolution and therefore the measured corrugation amplitudes, depend on the atomic configuration of the tip, the tip height, and the bias voltage.³³ A tunneling tip with fewer active tunnel site atoms averages over a smaller region of the surface, yielding better lateral resolution. In addition, the sample bias and tunneling current determine the distance of the tip from the surface, which also affects the area of the surface that contributes to the tunneling. Higher resolution is typically obtained for the low sample biases and higher tunneling currents where the tip is closer to the surface, sampling a higher electron density. In addition, a smaller STM tip close to the surface can observe increased short-wavelength contributions to the corrugation as the tunneling electrons are effectively contained within a smaller area of the sample. Scanning-tunneling-microscopy corrugations will generally be correct for wavelengths larger than the tip (typically a 1–3 atom cluster). Occasionally strange results can be obtained if the tip atoms have very directional bonding or low densities of states near the Fermi level, but such problems can be dealt with by repetition and proper attention to tip cleanliness. Various voltage and tip size effects can be observed in the STM topographs presented earlier. Helium scattering, of course, has the advantage of always using the same sized probe—a single helium atom.

Another source of difficulty with STM is thermal drift in the microscope and slow, history dependent terms in the piezoelectric actuators. Nonlinearities in the piezos

can result in 10% uncertainties in measured dimensions unless great care is taken. Thermal drift of the microscope can dramatically distort the geometry of some images, especially large ones, where it can take hundreds of seconds to acquire an image. While such a drift may be corrected without making a prior assumption about the image, residual errors due to changing drift rates or interactions with piezoelectricities result in geometric uncertainties on the level of a few percent. If an underlying lattice is visible, as is sometimes the case with a partially reacted surface, precise measurements may be made by comparing with the underlying lattice. However, in the present experiments, we were never able to image the copper lattice in the nominally unreacted areas, despite being able to image it on the clean crystal.

At first glance, helium scattering is quite different from STM as it is a diffractive technique. Typically, when one refers to the resolution of a HAS apparatus, one asks about the ability of the system to distinguish long-range periodicities. This lateral resolution of a helium diffractometer is determined by the beam energy, energy spread, angular divergence of the beam, and angular acceptance of the detector. In the lower incident-atom energy range, the resolution is restricted by the energy resolution of the helium beam, as clustering of the helium atoms occurs in the nozzle. In the higher-energy range, the angular separation between the diffraction peaks is reduced and the lateral resolution, transfer width, or coherence length is typically restricted by the angular acceptance of the detector. In most cases, the angular acceptance of the detector and the divergence of the beam are restricted by the signal level required to construct the diffraction pattern. At present, the energy resolution of the helium scattering is limited by the current beam technology.³⁴

If, however, one wishes to discuss the resolution of helium-atom scattering, in a sense that is directly analogous to the resolution of an STM apparatus, one does not need to consider the above factors. The short-range resolution is determined only by the accuracy to which one can measure the larger (well-spaced) diffraction intensities and the number of Fourier components one is able to identify within the corrugation of the surface unit cell. Typically then, for the weakly corrugated surfaces, the corrugation is established by comparing calculated with experimentally observed intensities.

Some qualitative similarities between the He and STM corrugations can be immediately implied, without sophisticated calculations of diffracted intensities.

(i) Both techniques see (5×3) or, more accurately, (5×13) periodicities. However, helium scattering can see evidence of longer-range periodicities, whereas the limited linearity on STM topographs restricts the ability to determine long-range periodicities accurately.

(ii) Neither STM nor HAS was able to see periodicities associated with the copper atoms in the hexagonal overlayer. These atoms were not resolved in the STM images. In the HAS diffraction pattern it is not possible to identify out of plane diffraction features that might be associated with a strong structure factor produced by an hexagonal overlayer of lattice parameter $\sim 2.56 \text{ \AA}$.

(iii) High-resolution STM topographs contain spatial frequencies away from the principle symmetry directions. These correspond directly to the Si hexagonal overlayer, with lattice parameter $\sim 4.43 \text{ \AA}$. There is little direct evidence for similar out-of-plane periodicities in the diffracted helium intensities. Apparently the helium atoms cannot easily "resolve" the Si atoms within the (5×3) unit cell, perhaps because the He interacts in a range much further from the surface plane than the closest range of the STM tip.

The limited energy range available for thermal energy helium-atom scattering experiment effectively restricts the distance to which the helium atoms can approach the surface, reducing the amplitude of the corrugations that can be probed. This is one of the reasons why thermal energy helium scattering observes little or no corrugation on low index, clean, metal surfaces, while a low noise STM can observe a corrugation on the same surface.

VI. DISCUSSION

An increase in upper layer density, of order 20%, is associated with the formation of an hexagonal overlayer while maintaining identical, in plane, nearest-neighbor distances. A further increase in density follows a 3.77% uniaxial compression and the formation of a quasihexagonal overlayer with an exact (5×1) registry on the fcc(001) substrate, as occurs in the case of Ir(001). The need for an increase in density is assumed to be the driving force for these reconstructions.^{35,36} It can be explained in terms of a nonoptimum local electron density produced by truncation of the bulk. Although such a (5×1) overlayer is in perfect registry with the substrate there is clearly a balance of factors producing this result. Perfect registry with the substrate may give a net lowering of surface free energy but the uniaxial compression results in bond angles that do not have the ideal 120° value.

The structure we propose for the Cu_2Si hexagonal overlayer is subtly different from a uniaxially compressed 5×3 arrangement. Figure 4 shows that the surface is also compressed in the $x3$ (or, equivalently, the $x13$) direction. Thus, the overlayer is compressed in both x and y directions. The compression in the $x3$ direction amounts to 3.85% and is close to the 3.77% compression in the $x5$ direction. The biaxial compression produces a further increase in density at the surface compared with a simple 5×3 overlayer while giving almost perfect hexagonal coordination of the surface atoms.

It is apparent that the driving force for moving from an ideal (5×3) overlayer to the observed structure is twofold: (a) a need for further compression and density increase in the overlayer and (b) the tendency to move to ideal 120° in plane bond angles. Finally, we need to mention the energy gain that can result from locking the overlayer in registry with the substrate every (13,1) substrate positions.

The rotation of an overlayer, for the optimization of strong attractive substrate interactions, with overlayer atoms, was first developed by McTague and Novaco.³⁷ Their model concerned the rigid rotation of an overlayer

only. In the present case we have observed a 0.73° rotation of one axis of the near hexagonal overlayer [which facilitates the (13,1) registry]; however, we have been careful to emphasize that there is no evidence for rotation of the second hexagonal axis. An alternative structure, which would be very close to locking in, follows from a uniform rotation of 0.73° and might be anticipated from the model of McTague and Novaco. Approximately, this would be described in matrix notation by the following:

$$\begin{bmatrix} 13 & 1 \\ -3 & 5 \end{bmatrix}.$$

A very small hexagonal bond angle distortion would be required for this exact structure. (A 120° bond angle is increased only slightly to 120.23° .) We believe that the rotated structure is extremely close to that proposed for the stable Pt(001) hex $R0.73^\circ$ phase. Investigation of the Pt(001) system¹⁸ also shows additional higher-order commensuration, similar to those seen for the Cu_2Si overlayer.

Our results rule out a simple rotation of the hexagonal surface mesh. The Cu_2Si overlayer exhibits a net shearing of a nearly ideal hexagonal overlayer. Bond angles are distorted from 120° to 120.43° . Given the above argument for the absence of bond angle strain in the simple rotated phase, it is surprising to us that the Cu_2Si overlayer does not behave in a similar fashion to the Pt. One could even have anticipated that, due to the directionality expected in a Cu to Si bond, there would have been a stronger driving force for maintaining 120° bond angles than in the purely metallic Pt system. It is clear, however, that an accurate theoretical modeling of this system must include many factors. The classic one-dimensional (1D) Frenkel-Kontorova model for an overlayer on a substrate³⁸ looks at the balance of energy variations produced by overlayer to substrate interaction with the energies gained in producing nonuniform overlayers involving model linear spring constants. Clearly the analogous 2D model for the Cu_2Si overlayer must include different interaction energies for Cu and Si with the substrate Cu lattice and, second, both lateral and tangential spring constants must be invoked to describe correctly the effect of overlayer shearing.

Rumpling of the overlayer, or Cu_2Si carpet, may be a significant factor in producing substantial strain changes. If we assume that the nuclear positions follow approximately the $5\times$ corrugation observed with the STM, we can calculate out-of-plane bond bend angles to be of order 10° . Bonds in the $5x$ direction would also be stretched by 1%, relative to bonds in a strictly flat overlayer. While there is no simple relationship between cor-

rugations at the fringes of the electron distribution and nuclear positions, the data certainly suggest substantial three-dimensional effects that would not be modeled in a strictly two-dimensional calculation.

The structure we propose for the Si/Cu(001) system has a remarkable similarity with the Cu/Si(111) system.⁹ Both adopt a locally hexagonal Cu_2Si planar overlayer that is restricted to a thickness of one atomic layer. The Cu-Si bond length in these two systems is also very similar: 2.46 Å in the present work compared with 2.49 Å in the Cu/Si(111). However, the mechanism for strain relief of the misfit between overlayer and substrate is quite different. In Cu/Si(111) strong directional bonds exist between the substrate and Si atoms in the overlayer. The result is an arrangement of small domains with a 5.55×5.55 structure. The domains are separated by distinct domain walls. The present work shows that, in the case of Si/Cu(00), the hexagonal Cu_2Si has long-range structural integrity and is more nearly like a floating incommensurate overlayer.

VII. CONCLUSION

In this paper, we have presented helium scattering and scanning-tunneling-microscopy results for the 5×3 silicon on the copper(001) structure. Both helium scattering and STM display the same surface periodicities, although in the case of STM, the surface structure can be observed directly, albeit less accurately. The helium scattering results show that the silicon atoms have been incorporated into the copper surface, with a rotation of one overlayer lattice vector of 4.4° and a high-order commensuration of the other surface-lattice vector. The STM results show that the surface has a hexagonal overlayer structure with a Cu_2Si stoichiometry. The rotation of one surface-lattice vector is produced by a shearing of the hexagonal overlayer of 0.73° with respect to the copper substrate and is accompanied by a contraction of the surface interatomic distance by approximately 4% from the bulk copper interatomic distance. The high-order commensuration in the " $5a$ " surface lattice vector is due to a very slight expansion of the near ideal hexagonal structure with respect to perfect 5 times registry with the square copper(001) substrate. By incorporation of Si into the surface plane, the surface layer atomic density is increased by a total of 27.6% with respect to the truncated Cu(001) surface. In the study presented here, the real-space imaging of STM has complemented the reciprocal space imaging of helium scattering, permitting a comprehensive structural study of the 5×3 copper(001)-silicon surface.

*Present address: Max-Planck-Institut für Strömungsforschung, Bunsenstrasse 10, D-37073 Göttingen, Federal Republic of Germany.

†Permanent address: Department of Chemistry, University of York, York YO1 5DD, U.K.

¹D. R. Heslinger, H. H. Weitering, D. P. van der Werf, T. M. Klapwijk, and T. Hibma, *Phys. Rev. Lett.* **64**, 1589 (1990).

²M. O. Aboelfotoh, A. Cross, B. G. Svensson, and K. N. Tu, *Phys. Rev. B* **41**, 9819 (1990).

³S. H. Corn, J. L. Falconer, and A. W. Czanderna, *J. Vac. Sci.*

- Technol. A **6**, 1012 (1988).
- ⁴M. Mundschaue, E. Bauer, W. Teliaps, and W. Swiech, *J. Appl. Phys.* **65**, 4747 (1989).
- ⁵H. Kemmann, F. Müller, and H. Neddermeyer, *Surf. Sci.* **192**, 11 (1987).
- ⁶D. D. Chambliss, T. N. Rhodin, and R. V. Kasowski, *J. Vac. Sci. Technol. A* **6**, 1499 (1988).
- ⁷S. A. Chambers, S. B. Anderson, and J. H. Weaver, *Phys. Rev. B* **32**, 581 (1985).
- ⁸R. B. Doak and D. B. Nguyen, *Phys. Rev. B* **40**, 1495 (1989).
- ⁹J. Zegenhagen, E. Fontes, F. Grey, and J. R. Patel, *Phys. Rev. B* **46**, 1860 (1992).
- ¹⁰L. H. Dubois and R. G. Nuzzo, *Langmuir* **1**, 663 (1985).
- ¹¹E. M. McCash, M. A. Chesters, P. Gardener, and S. F. Parker, *Surf. Sci.* **225**, 273 (1990).
- ¹²B. C. Wiegand, S. P. Lohokare, and R. G. Nuzzo, *J. Phys. Chem.* **97**, 11 553 (1993).
- ¹³A. P. Graham, W. Allison, and E. M. McCash, *Surf. Sci.* **269/270**, 394 (1992).
- ¹⁴A. P. Graham, Ph.D. thesis, University of Cambridge, 1993.
- ¹⁵R. Campargue, *J. Phys. Chem.* **88**, 4466 (1984).
- ¹⁶J. E. Griffith and G. P. Kochanski, *Annu. Rev. Mater. Sci.* **20**, 219 (1990).
- ¹⁷K. H. Rieder and T. Engel, in *Structural Studies of Surfaces*, edited by K. Heinz *et al.*, Springer Tracts in Modern Physics Vol. 91 (Springer, Berlin, 1982), p. 55.
- ¹⁸K. Kuhnke, K. Kern, G. Comsa, and W. Moritz, *Phys. Rev. B* **45**, 14 388 (1992); Klaus-Eberhard Kuhnke, Ph.D. thesis, Institut für Grenzflächenforschung und Vakuumphysik, Jülich, GmbH, 1991.
- ¹⁹P. Heilmann, K. Heinz, and K. Müller, *Surf. Sci.* **83**, 487 (1979).
- ²⁰M. A. van Hove, R. J. Koestner, P. C. Stair, J. P. Bibérian, L. L. Kesmodel, I. Bartos, and G. A. Somorjai, *Surf. Sci.* **103**, 189 (1981).
- ²¹N. Bickel and K. Heinz, *Surf. Sci.* **163**, 435 (1985).
- ²²K. H. Rieder, T. Engel, R. H. Swendsen, and M. Manninen, *Surf. Sci.* **127**, 223 (1983).
- ²³J. F. Wendelken and D. M. Zehner, *Surf. Sci.* **71**, 178 (1987).
- ²⁴D. F. Ollis and M. Boudart, *Surf. Sci.* **23**, 320 (1970).
- ²⁵C. M. Friend, J. G. Serafin, E. K. Baldwin, P. A. Stevens, and R. J. Madix, *J. Chem. Phys.* **87**, 1847 (1987).
- ²⁶L. H. Dubois and R. G. Nuzzo, *Surf. Sci.* **149**, 133 (1985).
- ²⁷G. Binnig and H. Rohrer, *Rev. Mod. Phys.* **59**, 615 (1987).
- ²⁸A. P. Graham *et al.* (unpublished).
- ²⁹N. Esberg and J. K. Norskov, *Phys. Rev. Lett.* **45**, 807 (1980).
- ³⁰J. Tersoff, M. Cardillo, and D. Hamann, *Phys. Rev. B* **32**, 5044 (1985); J. Tersoff and D. Hamann, *ibid.* **31**, 805 (1985).
- ³¹J. F. Annett and R. Haydock, *Phys. Rev. Lett.* **53**, 838 (1984).
- ³²Y. Imry, in *Directions in Condensed Matter Physics: Memorial Volume in Honor of Shangkeng Ma*, edited by G. Grinstein and G. Mazenko (World Scientific, Singapore, 1986), p. 101; R. Landauer, *Z. Phys. B* **68**, 217 (1987).
- ³³J. Tersoff and D. R. Hamann, *Phys. Rev. B* **31**, 805 (1985).
- ³⁴D. R. Miller, in *Atomic & Molecular Beam Methods*, edited by G. Scoles (Oxford University Press, New York, 1988), p. 14.
- ³⁵R. J. Needs, M. J. Godfrey, and M. Mansfield, *Surf. Sci.* **242**, 215 (1991).
- ³⁶J. G. Chen, S. Lehwald, G. Kisters, E. Preuss, and H. Ibach, *J. Electron. Spectrosc. Relat. Phenom.* **54/55**, 405 (1990).
- ³⁷J. P. McTague and A. D. Novaco, *Phys. Rev. B* **19**, 5299 (1979).
- ³⁸Y. I. Frenekl and T. Kontorova, *Zh. Eksp. Teor. Fiz.* **8**, 1340 (1938).

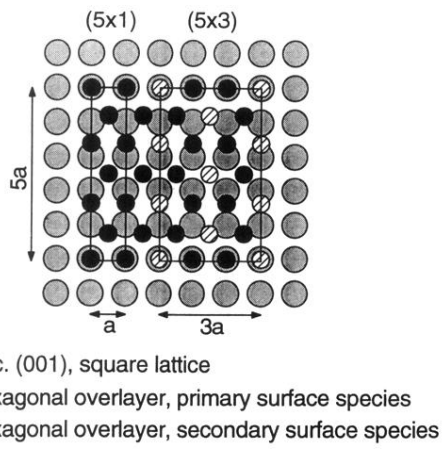


FIG. 3. Schematic representation of the hexagonal (hex) reconstruction on a square substrate. The hexagonal lattice almost matches with the square lattice after five lattice spacings. Hence a $5a$ periodicity would be observed by LEED and helium scattering. The $\sim 3a$ periodicity can be constructed by replacing every third surface atom with a different atomic species as shown.

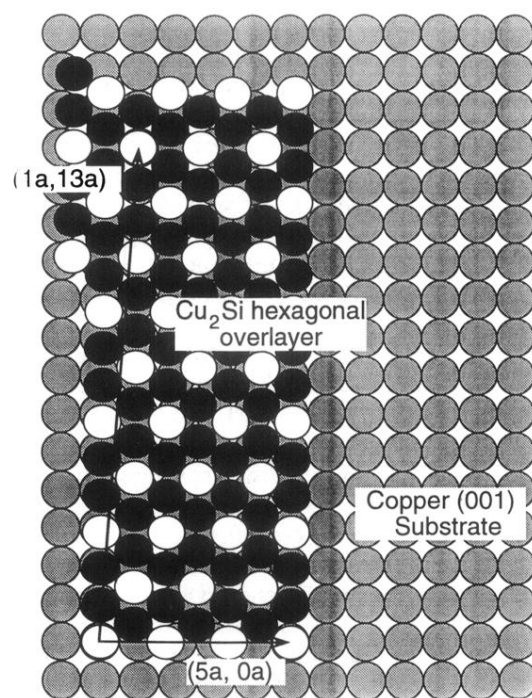


FIG. 4. Schematic diagram showing the proposed structural model of the surface layer together with the origin of the $13a$ periodicity and the 4.4° rotation. Note that the $5a$ direction is *not rotated* with respect to the copper substrate.

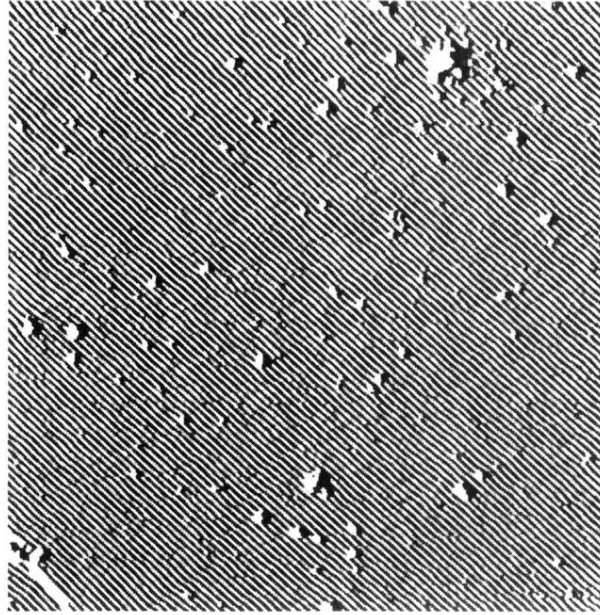


FIG. 5. A topograph of the surface following silane exposure to saturation at 420 K. The image was taken at a tunneling current of 0.2 nA and a sample bias of +3.0 V. The topograph is approximately 1160 Å across and has not been corrected for thermal drift of the STM during measurement. The topograph shown is the first derivative of the height data *across* the picture, i.e., dz/dx , where the height data has been convoluted with a 3.0-Å-wide Gaussian smoothing function before taking the derivative. Regions of positive slope are shown as bright, whereas regions of negative slope are shown as dark. The topograph shows one domain of the copper-silicon overlayer extending 1500 Å. The small islands on the topograph are probably copper that has been deposited from the tunneling tip.

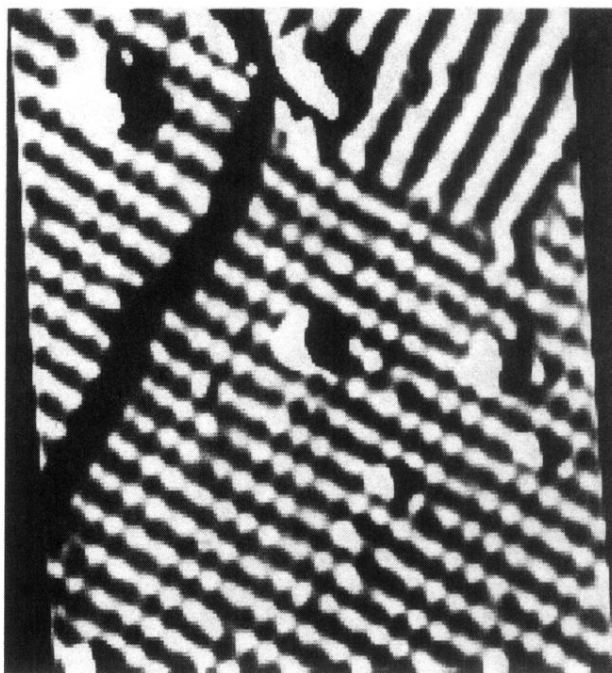


FIG. 6. A topograph of the surface following silane exposure to saturation at 420 K. The image was taken at a tunneling current of 0.1 nA and a sample bias of +2.0 V. The topograph is approximately 190 Å across and has been corrected for thermal drift of the STM during measurement. The topograph shown is the first derivative of the height data across the picture, i.e., dz/dx , where the height data has been convoluted with a 0.5-Å-wide (sigma) Gaussian smoothing function before taking the derivative. Regions of positive slope are shown as bright, where as regions of negative slope are shown as dark. The strongest corrugation on the copper-silicon structure is the $5a$ periodicity (stripes). Within each strip, the $3a$ periodicity can be seen, with a $13a$ periodicity observed as a modulation of the $3a$ periodicity height along the stripe. The dark band in the top left-hand corner of the topograph is a surface step.

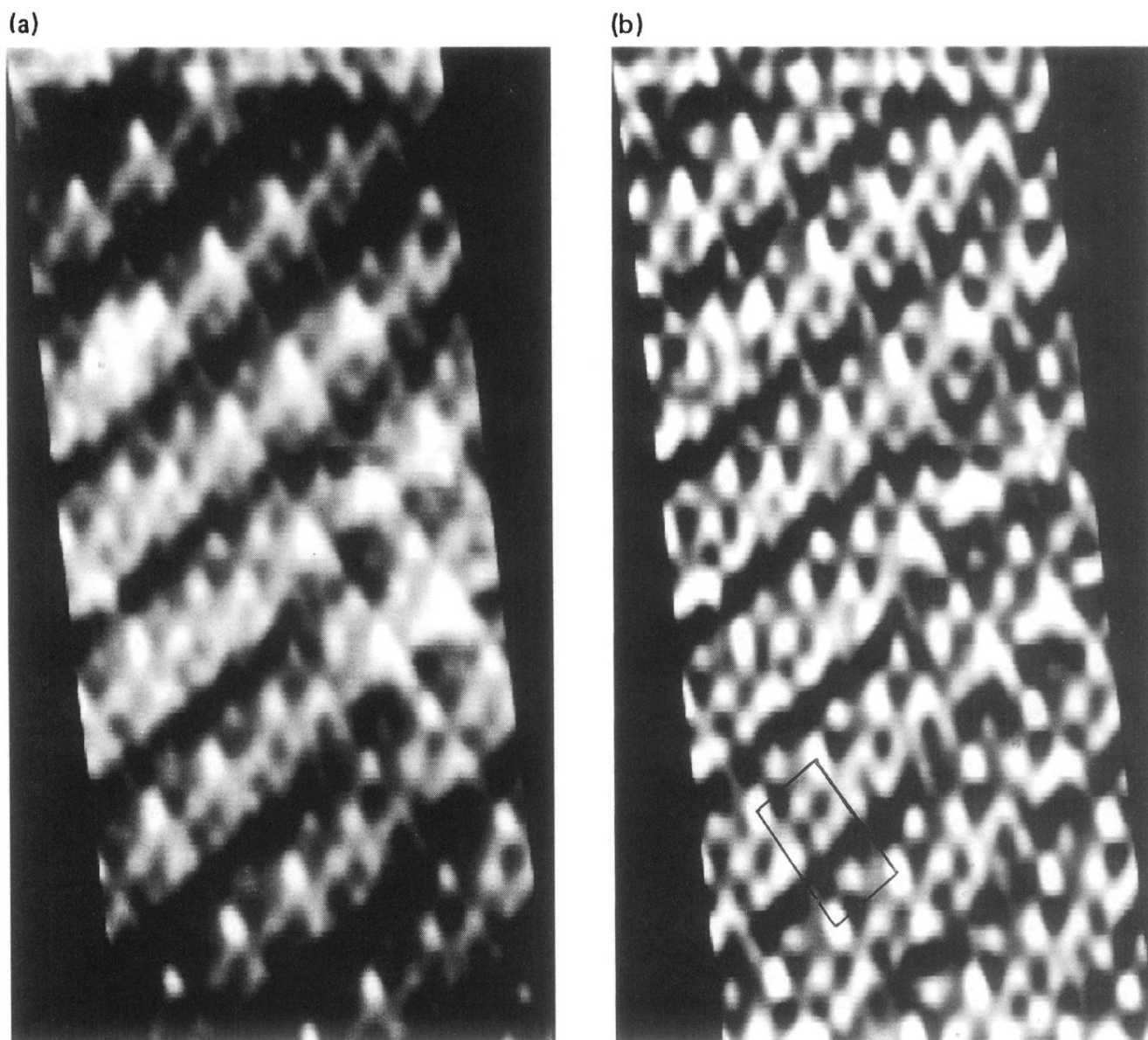


FIG. 7. A topograph of the surface following silane exposure to saturation at 420 K. The image was taken at a tunneling current of 1.0 nA and a sample bias of +0.5 V. The topograph is approximately 46 Å across and has been corrected for thermal drift. The most probable fit plane to the height data has been subtracted, and the data presented in two ways: (a) with the brightness representing the height, emphasizing the long-wavelength corrugations (5×3), and (b) with the brightness representing the local height (height relative to a 2-Å Gaussian-weighted average of the vicinity). The 5×3 unit cell is shown on the latter topograph. The highest topographic features on the surface lie in sites consistent with the minority surface species in a hexagonal overlayer structure. Hence the high features can be assigned to silicon atoms in the overlayer.

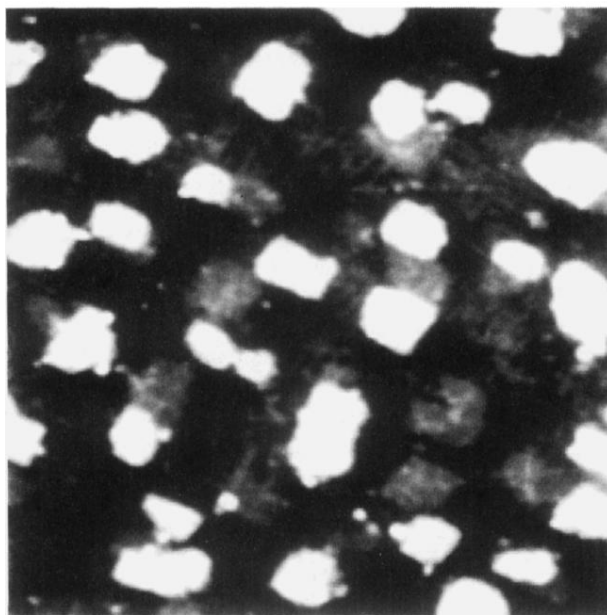


FIG. 8. A surface topograph following saturation silane exposure at 300 K. The image was taken at a tunneling current of 0.2 nA and a sample bias of 1.0 eV. The topograph is approximately 1050 Å across by 800 Å high and has not been corrected for thermal drift of the STM during measurement. The height data has been convoluted with a 1-Å-wide Gaussian smoothing function. The topograph shows part of a single terrace. The highest features on the terrace are the islands formed from the excluded copper.

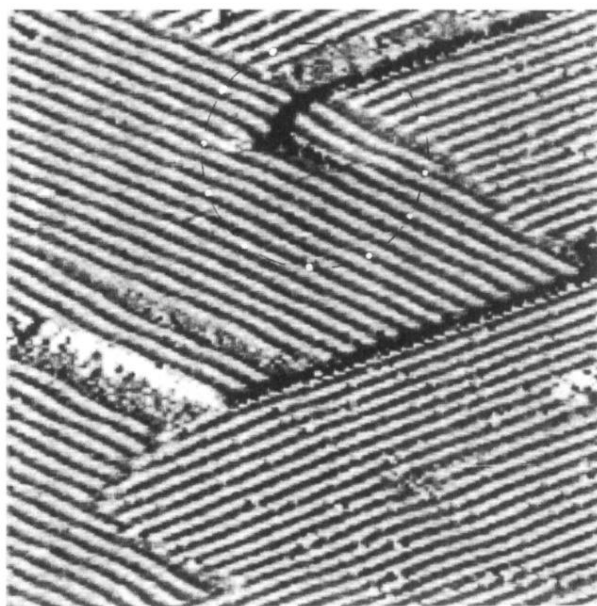


FIG. 9. A topograph of the surface following 8 L silane exposure at 420 K. The image was taken at 0.25 nA and +0.5 V. The topograph is approximately 280 Å across by 280 Å high and has not been corrected for thermal drift. The height data have been convoluted with a 0.5-Å-wide Gaussian smoothing function. A screw dislocation is faintly circled at the top center of the topograph. Note the minimal distortion of the overlayer lattice around the dislocation.